2013 IREP Symposium-Bulk Power System Dynamics and Control -IX (IREP), August 25-30, 2013, Rethymnon, Greece

Applying stochastic optimal power flow to power systems with large amounts of wind power and detailed stability limits

Camille Hamon
Electric Power Systems
Royal Institute of Technology

Magnus Perninge
Department of Automatic Control
Lund University

Lennart Söder
Electric Power Systems
Royal Institute of Technology

Abstract

Increasing wind power penetration levels bring about new challenges for power systems operation and planning, because wind power forecast errors increase the uncertainty faced by the different actors. One specific problem is generation re-dispatch during the operation period, a problem in which the system operator seeks the cheapest way of re-dispatching generators while maintaining an acceptable level of system security. Stochastic optimal power flows are re-dispatch algorithms which account for the uncertainty in the optimization problem itself.

In this article, an existing stochastic optimal power flow (SOPF) formulation is extended to include the case of non-Gaussian distributed forecast errors. This is an important case when considering wind power, since it has been shown that wind power forecast errors are in general not normally distributed. Approximations are necessary for solving this SOPF formulation. The method is illustrated in a small power system in which the accuracy of these approximations is also assessed for different probability distributions of the load and wind power.

Introduction

In recent years, large investments have been made in wind power, and this trend is expected to continue in the coming decades. Integrating more wind power in the production mix offers great opportunities for the society, such as reducing greenhouse gas emissions and the dependence on foreign fuel. Large wind power penetration does, however, require changes in the way power systems are planned and operated [1].

For the operation of power systems, frequency control schemes are crucial for ensuring the balance between the electric demand and the production. They enable system operators to re-dispatch the production either automatically or manually during real-time operations to follow the load variations. With wind power, these frequency control schemes must not only meet the uncertainties of the load but also those of the wind. Hence, using the frequency control reserves in an optimal way requires designing generation re-dispatch algorithms which account for these uncertainties while ensuring a secure power system operation.

A secure operation is ensured if the power system is operated within stability limits beyond which the system would become unstable. Examples of stability limits are voltage stability limits, small-signal stability limits and line thermal limits. Operating the system within these limits means that the operating point must stay in a stable operation domain.

Traditional generation re-dispatch algorithms do not consider the whole range of the uncertainties. Rather, they ensure that only for a few possible outcomes of the uncertainties, the power system will be in the stable operation domain after any of some selected contingencies. Margins must then be added for power system operation to be reliable even in the cases unaccounted for in the re-dispatch.

Other approaches which account for the whole range of the uncertainty have been developed. Stochastic optimal power flows are such algorithms. They are formulated as minimization problems with probabilistic constraints and the re-dispatch cost as objective function [2]–[5]. They are solved considering the whole probability distribution function of the stochastic system parameters. In particular, in [5], a S-OPF formulation with one single constraint ensuring a minimum level of system security, defined as the probability of the system to remain stable, is presented, and a method to solve it is proposed. The stability constraint uses parametrizations of approximations of the stability boundary developed in [6].

These previous works have solved the S-OPF problem with normally distributed uncertainty. This is a common assumption for the distribution of load forecast errors. When considering wind power in the uncertainty, however, the normal distribution has been shown not to be adapted for modeling wind power forecast errors [7], [8]. Rather, the beta and hyperbolic distributions have been suggested as appropriate.

In this paper, we further develop the method for solving the S-OPF formulation in [5] in order to include uncertainty with other distributions than the Gaussian distribution. This allows for the inclusion of wind power into the uncertainty considered when solving stochastic optimal power flows.

The paper is organized as follows. In the first section, background about generation re-dispatch is given. Stochastic optimal power flows are presented in the second section. In

The financial support for this project from Vindforsk is greatly acknowledged.

978-1-4799-0199-9/13/ $31.00

the third section, the method to solve the S-OPF formulation from [5] is extended to include non-Gaussian distributed uncertainty. The third section ends with a summary of the method and of the improvements made compared to original method in [5]. Application to power system operations is discussed in the fourth section. In the fifth section, a case study is carried out that assesses the accuracy of the proposed method.

Background in optimal generation re-dispatch

Security-constrained optimal power flow

The traditional way of getting an optimal generation re-dispatch is to solve a security-constrained optimal power flow (SCOPF) problem [9]. The constraints to the SCOPF problem ensures that the optimal solution satisfies the so-called $N-k$ criterion, where k is the number of simultaneous contingencies that the system must be able to survive. Examples of contingencies are tripping of major transmission lines or loss of large generation units. SCOPFs are either preventive [9] or corrective [10]. In the preventive case, the optimal setting of the control variables remains unchanged in the post-contingency systems, and ensures that the system survives the contingencies. In the corrective case, the optimal setting of the control variables can be different in the post-contingency systems.

In the following, the preventive SCOPF will be considered. Let n_c be the number of selected contingencies, and let $i=0$ correspond to the pre-contingency case. Preventive SCOPF can be expressed as

$$\begin{aligned} \min_{u_0} \quad & C(x_0, \lambda_0, u_0) && \text{(1a)} \\ \text{s.t.} \quad & f_i(x_i, \lambda_i, u_0) = 0, \quad i = 1, \ldots, n_c, && \text{(1b)} \\ & h_i(x_i, \lambda_i, u_0) \leq 0, \quad i = 1, \ldots, n_c, && \text{(1c)} \end{aligned}$$

where $x \in \mathbb{R}^{n_x}$, $\lambda \in \mathbb{R}^l$ and $u \in \mathbb{R}^k$ are the state variables (such as voltage magnitudes and angles), the parameters – such as the active power consumption – and the control variables, respectively. The function $C\colon \mathbb{R}^{n_x} \times \mathbb{R}^m \times \mathbb{R}^{n_u} \to \mathbb{R}$ is the objective function to be minimized, $f\colon \mathbb{R}^{n_x} \times \mathbb{R}^m \times \mathbb{R}^{n_u} \to \mathbb{R}^{n_x}$ represents the power flow equations ensuring that the solution corresponds to a possible equilibrium, and $h\colon \mathbb{R}^{n_x} \times \mathbb{R}^m \times \mathbb{R}^{n_u} \to \mathbb{R}^{n_l}$ contains n_l operational constraints. The objective function is to minimize the operating costs in the pre-contingency system. The optimal preventive actions are given by the optimal solution $\hat{u}_0$.

Generation re-dispatch under uncertainty

A secure dispatch as given by SCOPF is secure only for the considered contingencies and operating conditions. Operating conditions refer to λ in the formulations above, which contains parameters not controllable by the system operators. Wind power and load are two examples of such parameters. When solving a SCOPF, the parameter λ is given a value which, according to the system operator, reflects the operating conditions for which the study is done (for example, peak load). These values can be obtained by forecasts. The shortcoming of such approaches is that it only considers a small amount of operating conditions. Today, system operators protect the system against risks associated with uncertainty by having some operational margins, see for example the Swedish example in [11]. Considering uncertainties directly when computing the optimal decisions would allow a more flexible and efficient use of the system resources.

Stochastic optimal power flows

Formulation

Stochastic optimal power flows (S-OPF) address the aforementioned shortcoming of the traditional approach, because they include the uncertainty in the optimization problem itself [2]. When considering continuous distribution functions of the parameters (such as the traditional Gaussian distribution for loads), the constraints must be changed from being deterministic to being probabilistic because the probability of violating the deterministic constraints is nonzero. Work on S-OPF includes [2]–[4], [12], [13]. A general formulation of a S-OPF problem is

$$\begin{aligned} \min_{u} \quad & \mathbb{E}\left[C(x, \lambda, u)\right] && \text{(2)} \\ \text{s.t.} \quad & P\left[h_i(x, \lambda, u) \leq 0\right] \geq 1 - \alpha_i, \quad i = 1, \ldots, n_h, && \text{(3)} \end{aligned}$$

where $\alpha_i > 0$ are small and n_h is the number of probabilistic constraints.

In [2], a S-OPF was formulated to maximize the power transfer over a set of buses with the constraint that the probability of the transfers across some bottlenecks to violate their limit is kept low.

In [5], [6], [14] a stochastic optimal power flow formulation for generation re-dispatch with stability constraint was developed. Voltage stability, small-signal stability and operational limits are taken into account. This formulation is

$$\begin{aligned} \min_{u \in U} \quad & C_G(u), && \text{(4a)} \\ \text{s.t.} \quad & \sum_{i=0}^{n_c} q_i P[\zeta \notin D_i(u)] \leq \alpha, && \text{(4b)} \end{aligned}$$

where $u \in U \subset \mathbb{R}^k$ are the control variables, $C_G(u)\colon \mathbb{R}^k \to \mathbb{R}$ is the cost associated with control $u \in U$, n_c is the number of contingencies, q_i is the probability that contingency i occurs, $\zeta \in \mathbb{R}^l$ are the stochastic system parameters (load and wind power for example), $D_i(u) \subset \mathbb{R}^l$ is the stable operation domain in $\mathbb{R}^l$ and $1-\alpha$ is the desired level of system security. The case $i=0$ corresponds to the pre-contingency system. Contingencies occur with a small probability so that $q_i \ll 1$ for $i = 1, \ldots, n_c$ and $q_0 \approx 1$.

Here, the control variables will be taken as the set points of the generators participating in the generation re-dispatch.

The optimal solution to (4) gives the cheapest generation re-dispatch which ensures that the probability of the system to leave the stable operation domain after none or any one of the n_c contingencies has happened is smaller than α. The quantity $1-\alpha$ can thus be seen as a level of system security. It is assumed that the re-dispatch orders will be carried out.

The aim of this paper is to further develop the method used in [5] to include non-Gaussian distributions of the uncertainty ζ when solving (4).

Power system modeling

In the S-OPF formulation in (4), the stable operation domains $D_i(u)$ must be characterized. The characterization depends on the power system models.

Power systems are usually modeled by a set of differential algebraic equations (DAE) of the form

$$\dot{x} = f(x, y, \lambda), \tag{5a}$$
$$0 = g(x, y, \lambda), \tag{5b}$$

where $x \in \mathbb{R}^{n_x}$ are state variables, $y \in \mathbb{R}^{n_y}$ are algebraic variables, and $\lambda \in \mathbb{R}^m$ are parameters. The parameters $\lambda \in \mathbb{R}^m$ include here both the control variables $u \in \mathbb{R}^k$ and the stochastic system parameters $\zeta \in \mathbb{R}^l$ so that $\lambda = \begin{bmatrix} u^T & \zeta^T \end{bmatrix}^T$. The smooth functions $f\colon \mathbb{R}^{n_x} \times \mathbb{R}^{n_y} \times \mathbb{R}^m \to \mathbb{R}^{n_x}$ and $g\colon \mathbb{R}^{n_x} \times \mathbb{R}^{n_y} \times \mathbb{R}^m \to \mathbb{R}^{n_y}$ are the differential and algebraic equations, respectively. Generators' internal voltages and speeds are examples of state variables. The algebraic variables include bus voltages and angles.

If the behavior of the system for a specific value of the parameters is of interest, the dependence on λ can be omitted:

$$\dot{x} = f(x, y), \tag{6a}$$
$$0 = g(x, y). \tag{6b}$$

Equilibria of the system are given by

$$\begin{cases} 0 = f(x, y, \lambda), \\ 0 = g(x, y, \lambda). \end{cases} \iff F(z, \lambda) = 0, \tag{7}$$

where $z \in \mathbb{R}^{n_z} = \begin{bmatrix} x^T & y^T \end{bmatrix}^T$, $n_z = n_x + n_y$ and $F\colon \mathbb{R}^{n_z} \times \mathbb{R}^m \to \mathbb{R}^{n_z}$ for the whole set of equations at equilibrium.

Switching devices need special attention for modeling. Automatic voltage regulators (AVR) switching between voltage and overexcitation control are examples of switching devices. Switching devices can be modeled by different equations, depending on the state of the device, which means that the sets of equations f and g change as well. Furthermore, the type of one variable (state or algebraic variable) can change depending on the state of the device, and this must be dealt with carefully in the system modeling. For example, when the field voltage of a generator is under voltage control, it is considered as a state variable, whose dynamics are described by an equation entering f. When it reaches the voltage regulator's limit, however, it becomes an algebraic variable defined by an equation in g. In [15], an appropriate steady-state model for this case was given. It is made of the following equations at equilibrium:

$$\psi(z, \lambda) = 0, \tag{8a}$$
$$f^{a,i}(z) \cdot f^{b,i}(z) = 0, \quad i = 1, \ldots, n_s, \tag{8b}$$
$$f^{a,i}(z) \geq 0, \quad i = 1, \ldots, n_s, \tag{8c}$$
$$f^{b,i}(z) \geq 0, \quad i = 1, \ldots, n_s, \tag{8d}$$

where n_s is the number of switching devices, $f^{a,i}$ is the equation of the field voltage of generator i under voltage control, $f^{b,i}$ is the equation of the field voltage of generator i under overexcitation control and $\psi : \mathbb{R}^{n_z+m} \to \mathbb{R}^{n_z+m-n_s}$ are all equations in $F(z, \lambda)$ except those representing the switching devices. Equation (8b) ensures that at least one of $f^{a,i}$ and $f^{b,i}$ is zero. Hence $F(z, \lambda)$ in (7) includes all equations in ψ and, for each switching device, the equations $f^{a,i}$ and $f^{b,i}$ that are equal to zero. Note that for a certain generator i, it can happen that both $f^{a,i}$ and $f^{b,i}$ are equal to zero.

Stability boundaries

The stable operation domains $D_i(u)$, $i = 0, \ldots, n_c$, are bounded by the stability boundaries $\Sigma_i(u)$ consisting of different smooth parts $\Sigma_{ij}(u)$, $j \in J_i$, each one of them corresponding to different types of stability limits, such as saddle-node bifurcations (SNB) [16], switching loadability limits (SLL) [17], Hopf bifurcations [18] (HB) and operational limits (OL) [19]. Hence, for one given state i, $i = 0, \ldots, n_c$, of the system (pre- or post-contingency state), the overall stability boundary $\Sigma_i(u)$ is in general not smooth. Two smooth parts $\Sigma_{ij}(u)$ intersect on a manifold of points, called corner points in [19]. Note that the stable operation domains $D_i(u) \subset \mathbb{R}^l$ in the space of stochastic system parameters ζ are restrictions of the stable operation domains $D_i \subset \mathbb{R}^m$ in the space of parameters $\lambda = (u, \zeta)$ for a given value of u. The same applies to the stability boundaries $\Sigma_i(u)$ and their smooth parts $\Sigma_{ij}(u)$ which are restrictions to the ζ space of stability boundaries in the λ space.

Each smooth part Σ_{ij} of a loadability surface Σ_i is a manifold of co-dimension one in the m-dimensional space of parameters. Each smooth part is characterized by a set of equations $\Psi^{\text{TYPE}}(z, \lambda, r)$ where TYPE is the type of stability limits of interest (such as SNB, SLL, HB and OL), $z = \begin{bmatrix} x^T & y^T \end{bmatrix}^T$ as above, and $r \in \mathbb{R}^t$ are additional variables necessary to characterize the surface. All points λ on the stability boundaries are equilibria of the system. Hence, (7) holds for all smooth parts and is included in the set of equations Ψ. In [6], the other equations included in Ψ for the four types of stability limits presented above (SNB, SLL, HB and OL) were given.

Solving the S-OPF problem

Approximating the stable operation domains

Solving problem (4) requires the knowledge of the stable operation domains, and, hence, of the stability boundaries, which are not known but can be computed pointwise by running, for example, continuation power flows (CPF). However, the process of computing many points on the stability boundaries in order to have a precise knowledge of it is time consuming and therefore cannot be performed close to real-time, which is the time horizon of interest when solving the generation re-dispatch problem for power systems operation. In [5], it was proposed to approximate the different smooth parts Σ_{ij} of the stability boundaries by second-order approximations developed in [6], [20]–[22].

The second-order approximations will be denoted Σ_{ij}^a where $i = 0, \dots, n_c$ is for the state of the system (pre- or post-contingency) and $j \in J_i$ is for the smooth part of the stability boundary Σ_i which is approximated. These second-order approximations can be defined as below, where a short review of the theory from [6] is given.

Consider one smooth part $\Sigma_{ij} \in \mathbb{R}^m$. Let $n_{ij}(\lambda_c^{ij})$ be the normal vector to Σ_{ij} at a point λ_c^{ij}. A basis $\{c_1, \dots, c_{m-1}\}$ for the tangent hyperplane $T_{\lambda_c^{ij}}\Sigma_{ij}$ can be computed using for example the Gram-Schmidt process. Let $C_{ij} = [c_1 \dots c_{m-1}]$. The second-order Taylor expansion of Σ_{ij} around the point λ_c^{ij} is given by $L_{ij} : T_{\lambda_c^{ij}}\Sigma_{ij} \to \mathbb{R}^m$, defined as

$$L_{ij}(x_c) = \lambda_c^{ij} + C_{ij}x_c + \tfrac{1}{2}\mathrm{II}_{ij}(x_c)n_{ij}(\lambda_c^{ij}), \tag{9}$$

where x_c is a displacement away from λ_c^{ij} in the tangent hyperplane, and II_{ij} is the second fundamental form of Σ_{ij} at λ_c^{ij} [23]. In the following, the subscripts and superscripts *ij* will sometimes be omitted for ease of notations. The second fundamental form is defined as

$$\mathrm{II}(x_c) = -\left\langle \mathrm{d}N_{\lambda_c}(x_c), x_c \right\rangle. \tag{10}$$

The map $\mathrm{d}N_c : T_{\lambda_c}\Sigma_{ij} \to T_{\lambda_c}\Sigma_{ij}$ is the Weingarten map [23] which is the differential of the Gauss map $N : \Sigma \to \mathbb{S}^{m-1}$ where $\mathbb{S}^{m-1}$ is the unit sphere in $\mathbb{R}^m$, i.e. the map that takes the point $\lambda \in \Sigma_{ij}$ to the normal vector $n(\lambda) \in \mathbb{S}^{m-1}$, of Σ_{ij} at λ. The Weingarten map measures how much the normal vector changes, thus giving a measure of the curvature of the surface.

Second-order approximations of the stability boundary are local approximations around the approximation points λ_c. The closer to λ_c the better we can expect the accuracy of the approximations to be. The choice of λ_c therefore influences the accuracy of the approximations in the entire parameter space. It was proposed in [6] that the approximation point on each smooth part Σ_{ij} be chosen as the solution to the following optimization problem:

$$\max_{\lambda} \quad \rho(\lambda) \tag{11a}$$
$$s.t \quad \lambda \in \Sigma_{ij}, \tag{11b}$$

where $\rho \colon \mathbb{R}^m \to \mathbb{R}$ is a so-called importance function. This optimization problem is solved in [6] by a predictor-corrector method. Examples of importance functions are the negative Euclidean norm and probability density functions describing the uncertainty on the stochastic system parameters ζ. Examples were given in [20] where a similar problem was solved.

Distance functions d_{ij} giving the signed distance from any point $(u, \zeta) \in \mathbb{R}^m$ in parameter space to the corresponding second-order approximation of the smooth part Σ_{ij} can then be defined. The distances are defined in the direction of the normal to the corresponding smooth part at the point λ_c on Σ_{ij} at which the second-order approximation was computed:

$$\begin{aligned} d_{ij}(\lambda) &= (L_{ij}(C^T(\lambda - \lambda_c)) - \lambda) \cdot n(\lambda_c) \\ &= (\lambda_c - \lambda) \cdot n(\lambda_c) + \tfrac{1}{2}\mathrm{II}(C^T(\lambda - \lambda_c)). \end{aligned} \tag{12}$$

Note that the distance functions are random variables since ζ, and thus λ, is a random variable corresponding to the stochastic system parameters. A distance $d_{ij}(\lambda)$ is negative if the point λ is beyond the corresponding smooth part Σ_{ij}. Hence, the point λ does not belong to the approximation of the stable operation domain $D_i(u)$ if at least one of the distances d_{ij} is negative, $j \in J_i$, that is if $\min_{j \in J_i} d_{ij}(u, \zeta) < 0$.

The S-OPF formulation in (4) can therefore be approximated by

$$\min_{u \in U} \quad C_G(u), \tag{13a}$$
$$\text{s.t.} \quad \sum_{i=0}^{n_c} q_i P\left[\min_{j \in J_i} d_{ij}(u, \zeta) < 0\right] \leq \alpha. \tag{13b}$$

It will be convenient in the following to express the distances as second-order polynomials in ζ [5]:

$$d(u, \zeta) = a(u) + b_i(u)\zeta^i + c_{ij}\zeta^i\zeta^j, \tag{14}$$

where the tensor notation (sum over repeated indices) has been used, and $a(u) \in \mathbb{R}$, $b(u) \in \mathbb{R}^l$ and $c \in \mathbb{R}^{l \times l}$. Note that the coefficient of the quadratic term c does not depend on u. The coefficient $a(u)$ is a quadratic polynomial in u, and $b(u)$ an affine function in u. The expression of these coefficients are given in Appendix.

Computing the value of the constraint and its derivatives

Further approximations are needed to solve (13) because no formula is known to compute the probability of the minimum of dependent random variables. In [5], a pairwise exclusion method is used to this purpose. It allows us to write the part of the constraint corresponding to each system state i as an expression in which only probabilities of one or two distance functions being negative appear. In the following, the index i corresponding to the state of the system will be omitted, and we write d_j for d_{ij}, the distance function corresponding to the second-order approximation of the j-th part of the stability boundary for the system in state i. Hence, with the method from [5], $P\left[\min_{j\in J} d_j(u,\zeta)<0\right]$ can be approximated by an expression containing only terms of one of the following two forms

$$p_j = P\left[d_j(u,\zeta)<0\right] \tag{15}$$

$$\text{or } p_{jk} = P\left[\begin{bmatrix} d_j(u,\zeta)\\ d_k(u,\zeta)\end{bmatrix} < \begin{bmatrix}0\\0\end{bmatrix}\right] \tag{16}$$

where $d_j(u,\zeta)$ and $d_k(u,\zeta)$ are distance functions of the form (14). In this pairwise exclusion method, the important case of SNB-SLL intersections must be handled differently than other. More detail about these intersections can be found in [22].

The marginal probability distributions of the uncertainty ζ (wind power and load at each injection point) are assumed to be known. In order to compute the probabilities of the forms (15) and (16), however, the cumulative distribution functions of the distance functions are needed. Since the distance functions are second-order polynomials of the uncertainty, it is not, in general, possible to get an analytical expression of these probability distributions. It is proposed here to approximate these probabilities by Edgeworth approximations.

In the original method presented in [5], such probabilities where estimated by assuming that the vector $[d_j \quad d_k]^T$ was Gaussian and by numerically computing the probability in (16). In general, however, single distance functions and vectors of such distance functions are not Gaussian, even if the uncertainty ζ has a Gaussian distribution. Wind power forecast error distributions are not Gaussian [7], [8] and therefore introduce further deviation from a Gaussian distribution in ζ and the distance functions through (14). Using Edgeworth approximations allows us to account for non-Gaussian vectors.

Edgeworth approximations Edgeworth approximations can be used in order to approximate cumulative distribution functions such as the ones in (15) and (16). In the following, the notations from [24, Chapter 5] are adopted. Let X be a multivariate random variable with mean μ and covariance matrix Σ, and consider the cumulative distribution function $\Phi(x)$ of a multivariate normal random variable with same mean and covariance matrix as X. Then, the cumulative distribution function F_X of X can be approximated in x by

$$F_X(x) \approx \Phi(x) + \eta^{ijk}F_{ijk}(x)/3! + \eta^{ijkl}F_{ijkl}(x)/4! + \ldots, \tag{17}$$

where the tensor notation (sum over repeated indices) has been adopted,

$$F_{ijk}(x) = (-1)^3\frac{\partial^3\Phi(x)}{\partial x^i\partial x^j\partial x^k}, \tag{18}$$

$$F_{ijkl}(x) = (-1)^4\frac{\partial^4\Phi(x)}{\partial x^i\partial x^j\partial x^k\partial x^l}, \tag{19}$$

and $\eta^{ijk}, \eta^{ijkl}, \ldots$ are so-called formal moments, and can be computed from the cumulants $\kappa^{i,j,k}, \kappa^{i,j,k,l}, \ldots$ of X. Usually, the following truncation is used:

$$\begin{aligned} F_X(x) \approx \Phi(x) &+ \kappa^{i,j,k}F_{ijk}(x)/3! + \kappa^{i,j,k,l}F_{ijkl}(x)/4! \\ &+ \kappa^{i,j,k}\kappa^{l,m,n}F_{ijklmn}(x)/72, \end{aligned} \tag{20}$$

where the η:s have been replaced by their expressions in term of the cumulants of X.

Application to the S-OPF problem The needed probabilities in (15) and (16) can be approximated by Edgeworth expansions of the type (20) by noting that $p_j = F_{d_j}(0)$ and $p_{jk} = F_{d_j,d_k}(0,0)$. The first four cumulants of all single and pairs of distance functions are needed to apply (20). Assuming that the cumulants of the uncertainty ζ are known (for example as given by forecasts), the problem of computing the cumulants of vectors of distance functions arises.

In [24, Section 3.4], formulas are given for the cumulants of polynomial transformations of random variables, such as the distance functions in (14). The formulas are given in Appendix and allow for the computation of the first four cumulants $\kappa_{d,1}, \kappa_{d,2}, \kappa_{d,3}$ and $\kappa_{d,4}$ of a vector of p distance functions of the form (14) given the first eight cumulants of the uncertainty ζ.

Using the pairwise exclusion method from [5] and Edgeworth approximations, the probabilities $P\left[\min_{j\in J} d_j(u,\zeta)<0\right]$ appearing in the constraint of the S-OPF formulation in (13) can be approximated by $\hat{p}^i$, for all system states i, $i=0,\ldots,n_c$, where $\hat{p}^i$ is a sum of terms computed from Edgeworth approximations.

The S-OPF formulation in (13) then becomes:

$$\min_{u\in U} \quad C_G(u), \tag{21a}$$

$$\text{s.t.} \quad \sum_{i=0}^{n_c} q_i\hat{p}^i(u) \le \alpha, \tag{21b}$$

This is a nonlinear constrained optimization problem. The Lagrangian is

$$\mathcal{L}(u,\gamma) = C_G(u) - \gamma\sum_{i=0}^{n_c} q_i\hat{p}^i(u), \tag{22}$$

where γ is the Lagrangian multiplier. From the analytical expressions of the $\hat{p}^i(u)$ as sums of terms computed from Edgeworth approximations, the first- and second-order derivatives $\nabla_u\mathcal{L}$ and $\nabla_{uu}\mathcal{L}$ of the Lagrangian can be obtained. The Karush-Kuhn-Tucker (KKT) conditions are used to find a local optimum to the problem [25].

Estimating the cumulants of the stochastic system parameters

In the method presented above, the cumulants of the distance functions are computed from the cumulants of the stochastic system parameters ζ, which are assumed to be known. In practice, load and wind power forecasts will be available, and the uncertainty ζ then corresponds to the forecast errors around the forecasted values. These forecast errors can be described as probability distributions. For instance, the load forecast errors are often taken as Gaussian distributed and several publications have shown that wind power forecast errors follow beta or hyperbolic distributions [7], [8].

Given these forecast error probability distributions, a large number of samples of ζ can be generated, from which the cumulants are estimated using standard statistical analysis software.

Summary of the proposed method and of the contributions

Using the S-OPF formulation in (21) for re-scheduling generation during operation requires two phases:

- Phase 1: compute the second-order approximations for the pre- and post-contingency systems.
- Phase 2: solve the S-OPF.

During phase 1, for each system state $i = 0, \ldots, n_c$, second-order approximations Σ_{ij}^a of the smooth parts Σ_{ij}, $j \in J_i$ of the stability boundary for this system state are computed. During this phase, the stochastic system parameters ζ are assumed to be distributed according to a probability distribution P_1. Distance functions d_{ij}, $j \in J_i$ are defined for each second-order approximation from (12).

During phase 2, the S-OPF problem in (21) is solved. Cumulants of all single and pairs of distance functions are needed in order to compute all $\hat{p}^i(u)$, $i = 0, \ldots, n_c$, using Edgeworth approximations. These cumulants are computed from the cumulants of the stochastic system parameters ζ, which are assumed to be distributed according to a probability distributions P_2. Note that P_2 can be different from P_1, since the S-OPF problem is solved after the second-order approximations have been computed, and, hence, a better knowledge of the distribution of ζ may be available.

Compared to the initial method in [5], the contribution of this paper is the use of Edgeworth approximations which account for non-Gaussian distributed vectors of distance functions. As explained above, accounting for non-Gaussian distributions is particularly important when wind power forecast errors are considered in the uncertainty. The computations of the required cumulants to be used in the Edgeworth approximations were explained in detail above.

Application to power systems operation

Phase 1 is the most-time consuming phase and cannot be performed during real-time operation. The second-order approximations are computed around approximation points on the actual stability boundary, which are found considering forecasts for the stochastic system parameters such as load and wind power. Phase 2, however, is performed in real-time when the system operator wants to re-schedule the generation. After solving the S-OPF problem, an optimal re-scheduling is obtained, but there is a delay before the re-scheduling orders are carried out. Hence, when phase 2 is performed, forecasts for the system parameters are also used, but, compared to phase 1, forecasts are done closer to the time at which the re-dispatch orders are fully enforced.

Since the second-order approximations are local approximations, the closer to the approximation points, the better the approximations. The approximation points are found by maximizing the importance function ρ in (11). Hence, better forecasts will improve the accuracy of the method, since the actual system parameters will then be close to the approximation points. It is therefore desirable to perform phase 1 as close as possible to the operating period. The forecasts used during phase 2 will be more accurate than those for phase 1 because they are performed closer to the time for which the system parameters are forecasted. It is thus important to note that the forecasts are different between phase 1 and phase 2.

This is depicted in Figure 1. Before the operating period, at $t = t_0$, the second-order approximations are computed using forecasts available at $t = t_0$ for the stochastic system parameters (forecasts **F1** in the figure). During the operating period, at $t = t_1$, the system operator solves the S-OPF problem, using updated forecasts **F2**, and sends re-scheduling orders according to the optimal solution. Later during the operating period, at $t = t_1 + \delta$, the re-scheduling orders will be fully carried out, δ time steps after the order was given at $t = t_1$.

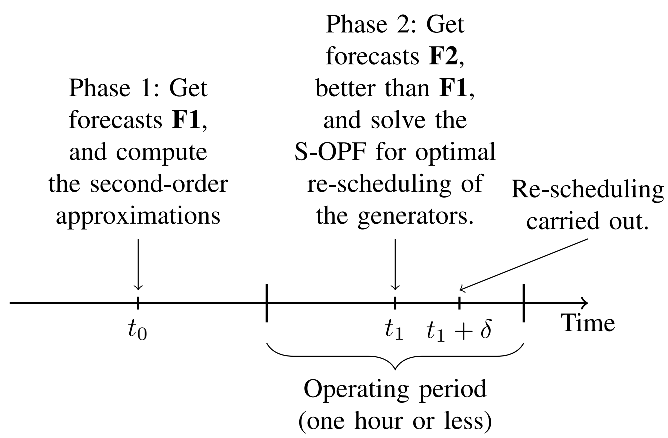

Fig. 1: The two phases in solving the S-OPF problem.

Case study

Problem description

We aim at assessing the accuracy of the overall method of solving (4), that is of using the approximation (21) instead of (4). We consider the power system from [19] in Figure 2. The system has three generators and one load.

Generator 1 is the only generator participating in primary frequency control while reserves can be activated discretely by re-dispatching generator 3. Generator 2 is a wind farm with installed capacity P_{inst}. Generators 1 and 3 must make up for both the wind and the load variations. When the system operator decides upon the optimal production level of generator 3, she must therefore take into account the uncertainty coming from both the wind and the load.

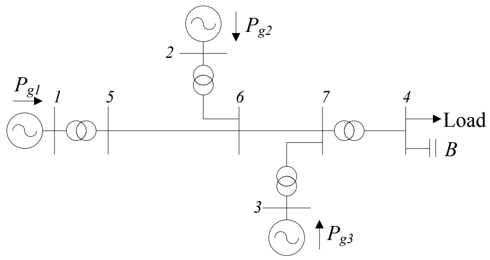

Fig. 2: Power system from [19].

The three generators are equipped with first-order automatic voltage regulators (AVR) with overexcitation limiters (OXL). These devices are modeled by the following equations

$$f^{a,i}(z) = E_{f,i} + K_i \left(V_{\text{ref},i} - V_i\right), \quad i \in \{1,2,3\} \tag{23}$$

$$f^{b,i}(z) = -E_{f,i} + E_{f,i}^{\text{lim}}, \quad i \in \{1,2,3\}, \tag{24}$$

where $f^{a,i}(z)$ and $f^{b,i}(z)$ were defined in (8), E_{fi} are the excitation field voltages, K_i the gains of the exciters, $V_{\text{ref},i}$ the terminal voltage references, V_i the terminal voltages and E_{fi}^{lim} the limits of the exciters.

All transformer ratios are set to 1. The load is assumed to have a constant power factor equal to $2/\sqrt{5}$, corresponding to $P_l = 2Q_l$, where P_l and Q_l are the active and reactive power consumptions of the load, respectively. Further details are given in Table I.

TABLE I: Power system details

$x_{15} = x_{26}$	$x_{37} = x_{47}$	x_{56}	x_{67}
0.032	0.016	0.12	0.005625
B	K_i	$V_{\text{ref,i}}$	E_{fi}^{lim}
0.25	100	1	2.5968

One contingency will be considered in addition to the base case (system without any contingency): Fault on the line $5-6$ corresponding to doubling the line impedance, which becomes $x_{56} = 0.24$.

Stability boundaries

The stability boundaries for these two cases (pre- and post-contingency) have been computed using continuation power flows and are plotted in Figures 3 and 4. Different colors correspond to different smooth parts, as explained above. The legends giving the types of the different smooth parts are presented in Tables II and III. The last two columns give the generators which are under OXL or on AVR. At an SLL, one of the generators is in both sets.

Scenarios

Recall from above that the S-OPF problem is divided in two phases: computing the second-order approximations before the operating period, using a forecast **F1**, and solving the optimization problem during the operating period, using a different forecast **F2**.

The load forecasts are here modelled by Gaussian distributions, and the wind power forecasts by beta distributions. The parameters of these distributions vary depending on which forecast is of interest. The load and wind power forecasts are $\mathcal{N}(\mu_i, \sigma_i^2)$ and $\beta(a_i, b_i)$, respectively, for forecast **Fi**, $i = 1, 2$. The wind farm is also characterized by its installed capacity P_{inst}. A scenario will therefore be a set of values μ_i, σ_i, a_i, b_i and P_{inst}. The different scenarios considered for this case study can be found in Table IV.

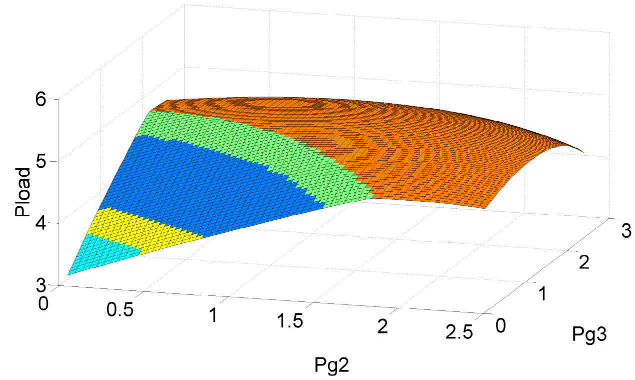

Fig. 3: Stability boundary of the base case system.

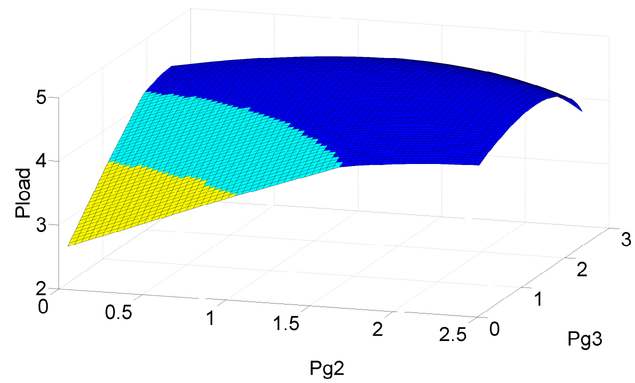

Fig. 4: Stability boundary of the system after contingency.

TABLE II: Smooth parts of the stability boundary of the base case system.

Color	Type	Generators on AVR	Generators under OXL
Orange	SLL	1,2	2,3
Green	SLL	2	1,2,3
Dark blue	SNB	2	1,3
Yellow	SLL	2,3	1,3
Light blue	SNB	2,3	1

TABLE III: Smooth parts of the stability boundary of the system after contingency.

Color	Type	Generators on AVR	Generators under OXL
Dark blue	SLL	1,2	2,3
Light blue	SLL	1,2	1,3
Yellow	SLL	1,2,3	1

TABLE IV: Definition of the scenarios with scenario 0 as base case. Only values different from the base case are shown for the other scenarios.

Scenario number	μ_i	σ_i	a_i	b_i	P_{inst} [p.u.]
0	**4.3**	**0.5**	**2**	**5**	**2.5**
1	3	–	–	–	–
2	3.5	–	–	–	–
3	3.5	–	7	7	–
4	3.5	–	20	50	–
5	3.5	–	50	50	–
6	–	–	20	50	–

The base case is scenario 0. The second-order approximations are computed using this scenario, i.e. scenario 0 gives the forecast **F1** used for seeking the most likely points around which the second-order approximations are computed. Then all scenarios are studied using these second-order approximations.

The coordinates of the points around which the second-order approximations of the different smooth parts were computed are given in Tables V. The coordinates are given in the (P_{g2}, P_{g3}, P_l) space. The colors correspond to the ones in Tables II and III.

TABLE V: Coordinates of the approximation points for each smooth part of the pre- and post-contingency stability boundary.

System	Color	P_{g2}	P_{g3}	P_l
Pre-contingency	Orange	0.65	1.53	4.96
–	Green	0.49	1.28	4.66
–	Dark blue	0.41	1.11	4.48
–	Yellow	0.26	0.57	3.86
–	Light blue	0.20	0.31	3.56
Post-contingency	Yellow	0.33	0.70	3.57
–	Light blue	0.53	1.27	4.26
–	Dark blue	0.58	1.35	4.38

With scenarios 0, 1 and 2, the effect of load forecast errors will be studied. Scenarios 3, 4, 5 and 6 will be used to study the effect of different parameters for the beta distribution. They can be compared to scenarios 0 and 2 which use the same beta distribution as for the computation of second-order approximations. In all scenarios, the probability of occurrence of the contingency is set to $q_1 = 0.02$ so that the probability of the base case is $q_0 = 0.98$.

Figure 5 shows the probability density functions for the beta distributions encountered in the scenarios. In the figure, the wind power capacity is assumed to be 2.5 p.u.

In Table VI, the mean, standard deviation, skewness and excess kurtosis of these two beta distributions, scaled for an installed capacity of 2.5 p.u., can be found. The skewness and excess kurtosis of a normal distribution are zero. For other distributions they can be used as measures of how much these distributions differ from the Gaussian distribution.

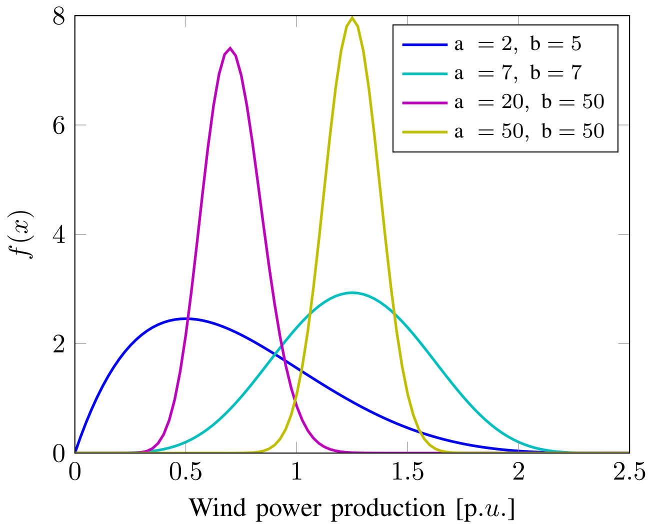

Fig. 5: Probability density functions f of Beta distributions $\beta(a, b)$ with different parameters a and b describing the wind power production from a wind farm with capacity 2.5 [p.u.].

TABLE VI: Statistical information for the beta distributions.

Scenario number(s)	a	b	Mean	Standard deviation	Skewness	Excess kurtosis
0, 1, 2	2	5	0.71	0.40	0.60	-0.12
3	7	7	1.25	0.32	0	-0.35
4, 6	20	50	0.71	0.13	0.22	-0.01
5	50	50	1.25	0.12	0	-0.06

Results

The problem in (21) is to be solved in the case where $u \in \mathbb{R}$ is the change in production from the base case in generator 3 and $\zeta = [P_{g2} \quad P_l]^T \in \mathbb{R}^2$ is the uncertainty due to forecast errors in the load and in the wind power production from the wind park in generator 2. The generation in generator 3 is therefore $P_{g3} = P_{g3}^0 + u$. In the following, we take $P_{g3}^0 = 0$ so that $P_{g3} = u$. The re-dispatch cost function $C_G(u)$ is assumed to be increasing with u. Considering the contingency described above, the problem becomes:

$$\min_{u \in \mathbb{R}} \quad C_G(u), \tag{25a}$$
$$\text{s.t.} \quad \hat{p}_{\text{fail}}(u) = q_0 \hat{p}^0(u) + q_1 \hat{p}^1(u) \leq \alpha. \tag{25b}$$

The probabilities of system failure for different values of P_{g3} are plotted in Figure 6. The probabilities have been computed both by the approximation method described above (solid lines in the figure), and by numerical integration (dotted lines). The latter value can be used as a reference to assess the accuracy of the approximation method and is calculated in the following way. For a given contingency and a specific value of $P_{g3}(u) = u$, let $(P_L(u), P_{g2}(u))$ be all points on the stability boundary for this value of u. Then

$$P\left[\zeta = [P_L \quad P_{g2}] \notin D(u)\right] = 1 - P\left[\zeta \in D(u)\right] \tag{26}$$

and

$$
\begin{aligned}
&P\left[\zeta=[P_L \quad P_{g2}] \in D(u)\right] \\
&=\int_{x=0}^{1}\left(\int_{z=-\infty}^{\hat{P}_l(u,x)} \phi(z)dz\right) f_X(x)dx \\
&=\int_{x=0}^{1} \Phi(\hat{P}_l(u,x)) f_X(x)dx
\end{aligned} \tag{27}
$$

where $\hat{P}_l(u,x)$ is the value of the load on the stability boundary when $P_{g3}=u$ and $P_{g2}=P_{\text{inst}}x$, ϕ and Φ are the probability density and cumulative density functions of the Gaussian distribution $\mathcal{N}(\mu_L,\sigma_L)$ describing the load, and f_X is the probability density function of $X=P_{g2}/P_{\text{inst}}$ which is beta distributed. The inner integration bounds $\hat{P}_l(u,x)$ are found by running continuation power flows, that is increasing P_l for the given u and $P_{g2}=P_{\text{inst}}x$ until reaching the stability boundary.

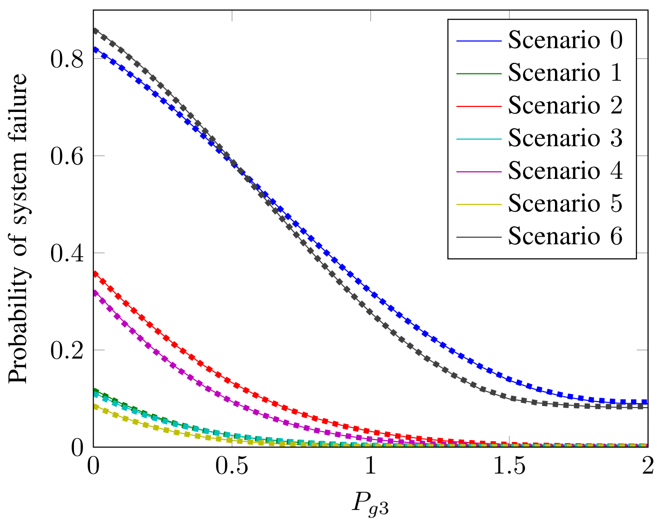

Fig. 6: Probability of system failure as a function of the production in generator 3. Solid lines give the estimations using the proposed method (second-order approximations and Edgeworth expansions). Dotted lines give the exact probability of system failure.

In Figure 6, the exact probabilities and their approximations are almost indistinguishable. It can also be observed that the larger the production in generator 3, the smaller the probability of the system to become unstable, as expected since power transfer from the remote generator 1 is then reduced. The optimal solution to the optimization problem is therefore the value of u for which the constraint is exactly equal to α, since it would cost more to ensure a value of the constraint strictly smaller than α.

The accuracy of the proposed method to solve the SOPF problem can be assessed by computing the error $\frac{p_{\text{fail}}-\hat{p}_{\text{fail}}}{p_{\text{fail}}}$, where $\hat{p}_{\text{fail}}$ is the estimated probability of system failure computed by the proposed method, and p_{fail} is the exact probability of system failure computed by numerical integration. The errors for each scenario are plotted in Figure 7 as function of the production in generator P_{g3}.

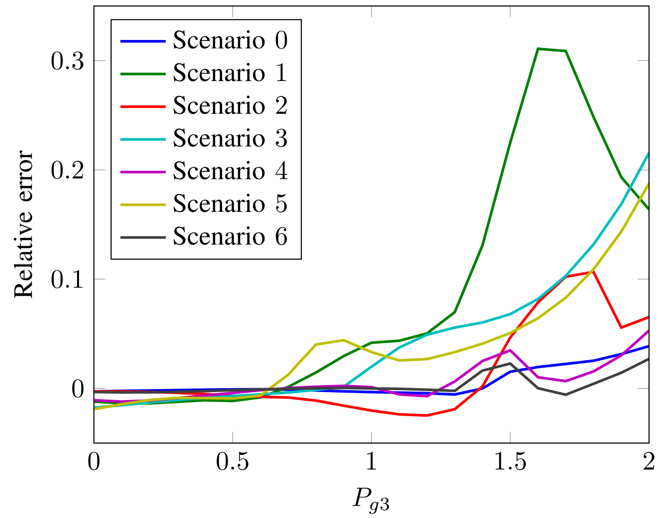

Fig. 7: Relative error $\frac{p_{\text{fail}}-\hat{p}_{\text{fail}}}{p_{\text{fail}}}$ as a function of the production in generator 3.

Discussion

Several approximations were necessary to obtain the SOPF formulation in (21) from the original one in (4):

- Second-order approximations of the stability boundary were used instead of the real ones. The second-order approximations are computed using scenario 0.
- The probability of the system to be outside the second-order approximations is computed by Edgeworth expansions.
- The cumulants of the uncertainty ζ are not known but estimated from a large number of samples of the ζ.

The error resulting from the last approximation can be reduced by increasing the number of samples. In the following, the impact of the first two approximations will therefore be emphasized. The total error due to these approximations are reflected in Figure 7. The relative error increases as the production in generator 3 increases. This decrease in relative accuracy can be explained partly because this region is far away from the approximation points (see Table V) and partly because the probability of system failure becomes very small as P_{g3} increases. To further investigate this, the relative errors are plotted against the exact probabilities of system failure (obtained by numerical integration) in Figures 8 and 9. It can be seen from Figure 8 that there is a trend of increasing relative error as the probability of system failure becomes smaller. This is further emphasized in Figure 9, where compared to Figure 8, only the cases in which the probability of system failure is smaller than 0.01 have been kept. It is seen clearly that in most cases, the relative error remains under 0.1, but increases above this value as the probability of system failure becomes smaller (under 0.002).

Scenarios 0, 1 and 2 differ in the average load given by the forecast. Scenario 1 has the largest peak in relative error (see

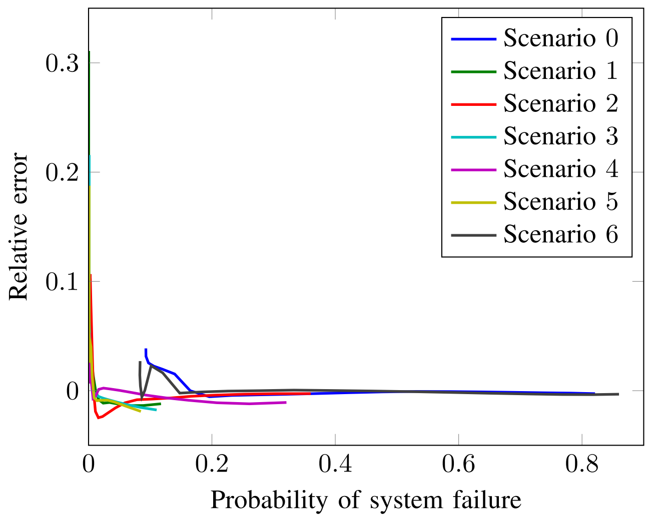

Fig. 8: Relative errors as functions of the probabilities of system failure.

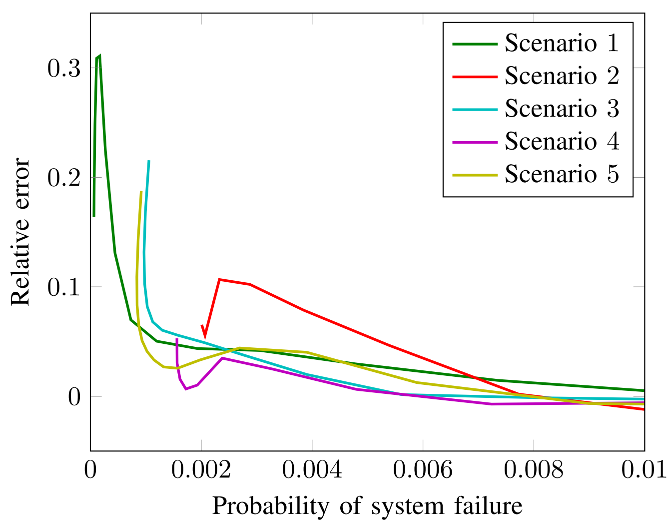

Fig. 9: Magnified parts of Figure 8: Relative errors as functions of the probabilities of system failure. Scenarios 0 and 4, not shown in the figure, have probabilities of system failure higher than 0.1 in all cases.

Figures 7 and 9), which can be explained both by the large error in load forecast (deviation from the base case scenario 0 used for computation of second-order approximation) and by the fact that the probability of system failure to be estimated becomes very small.

The load forecast error distributions are the same in scenarios 2 and 4, and but wind power forecast errors are modeled by two different beta distributions (see Table VI). The differences in these scenarios are the higher moments of the beta distributions. From Table VI, it can be seen that the beta distribution of scenario 4 is closer to a Gaussian distribution since both skewness and excess kurtosis are closer to zero compared to scenario 2. The absolute value of the relative error for scenario 4 is slightly larger than that for scenario 2 for probabilities of failures larger than 0.15 (compare the magenta and red curves in Figure 8). It becomes the opposite when the probabilities of system failure becomes smaller, with smaller relative errors for scenario 4 than for scenario 2 (see Figure 9). Scenario 2 uses the same beta distribution as the one used for computing the second-order approximations. It appears therefore that the accuracy of the Edgeworth approximations when probability distributions deviate too much from the normal distribution is the main source of error when estimating low probability of system failures.

However, this observation is not supported by the study of scenarios 3 and 5 which have different beta distributions with same mean, skewness of zero but different standard deviations and excess kurtosis. Figure 9 shows that the relative errors behave in a similar manner for these two scenarios although scenario 5 is closer to a normal distribution (lower absolute value of the excess kurtosis).

To investigate further the contribution of the different approximations, the total error can be broken down into two components: the error due to the second-order approximations and the error due to the other approximations, mainly Edgeworth expansions. This breakdown can be done as follows. The probability of system failure can be computed assuming that the second-order approximations are the real stability boundaries by using the same numeric integration method as in (27) and computing the inner integration bound $\hat{P}_l(u,x)$ as the point on the second-order approximation when generator 2 is producing $P_{g2} = P_{\text{inst}}$ and generator 3 $P_{g3} = u$. There is one such value $\hat{P}_l(u,x)$ for each smooth part, and it corresponds to the point $(P_{g2}, P_{g3}, \hat{P}_l(u,x))$ for which the distance function in (14) of this smooth part is zero. The point corresponding to the relevant smooth part for these values of P_{g2} and P_{g3} is then chosen as the inner integration bound. The corresponding probability of failure using the second-order approximations as actual stability boundary is denoted p^a_{fail}. The following two relative errors can now be computed:

1) $\frac{p_{\text{fail}} - p^a_{\text{fail}}}{p_{\text{fail}}}$: error due to the second-order approximations (see above for the definition of p_{fail}).
2) $\frac{p^a_{\text{fail}} - \hat{p}_{\text{fail}}}{p^a_{\text{fail}}}$: error due to the the other approximations (estimating the cumulants of the uncertainty ζ and using Edgeworth expansions, see above for the definition of $\hat{p}_{\text{fail}}$). Since the cumulants can be estimated accurately if enough samples of the uncertainty are used, this error is mostly due to Edgeworth approximations.

Figure 10 shows the breakdown of the total relative error into these two errors for each scenario. It shows that in all cases, the predominant term in the total error as P_{g3} increases far from the approximation points is the one associated with second-order approximations. For smaller values of P_{g3}, however, the error corresponding to using Edgeworth approximations can be predominant.

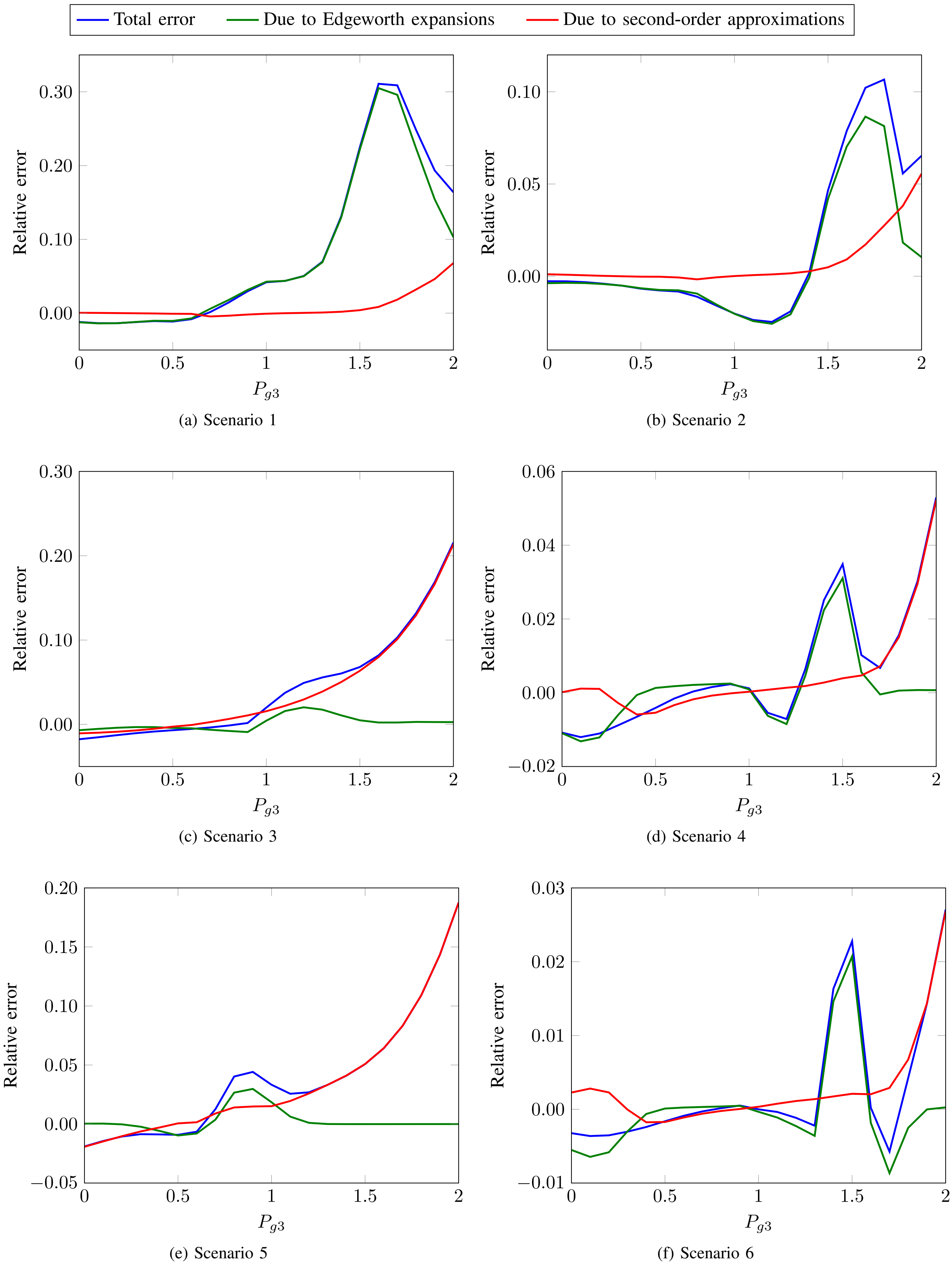

(a) Scenario 1
(b) Scenario 2
(c) Scenario 3
(d) Scenario 4
(e) Scenario 5
(f) Scenario 6

Fig. 10: Breakdown of the relative error for the seven scenarios.

Looking further at the error due to the second-order approximations, when P_{g3} increases, the valid smooth parts of the actual stability boundaries are the orange one in the base case (Figure 3) and the blue one in the post-contingency case (Figure 4). These two smooth parts' curvature change as P_{g3} increases, especially in the region where also P_{g2} is large (top-right hand corner in the figures). Since second-order approximations do not account for changes in the curvature, this impacts the accuracy of the approximations. Two solutions could be considered to enhance this accuracy:

1) Use more second-order approximations: for each smooth part, several second-order approximations could be computed, each valid for different parts of the smooth parts. The issue with this solution is the choice of the approximation points of the additional second-order approximations.
2) Use higher order approximations: third-order approximations of the stability boundaries could be used. Formulas for third-order approximations are given in [22]. Since only one third-order approximation would be computed for each smooth part, the method described above for identifying the best approximation points could still be used.

Conclusion

In this paper, a previous stochastic optimal power flow formulation for generation re-dispatch was further developed in order to be able to handle forecast errors which are not Gaussian distributed. It is important to consider non-Gaussian distributions in power systems with large amounts of wind power since it was shown that wind power forecast errors are typically not Gaussian distributed [7], [8]. The formulation is an optimization problem in which the cost of re-dispatch is minimized while keeping the probability of system failure low.

A method is proposed to solve the arising minimization problem. The method builds upon second-order approximations of the stability boundary and Edgeworth expansions to estimate the probability of system failure. The accuracy of the method is assessed in an illustrative example, and the obtained results show that the relative error due to the approximations is low, but increases as the probability of system failure to be estimated decreases. In future work, further assessments of the method should be carried out to study how the method scales in larger power systems. Attention should be given to the behavior of the method to estimate low probabilities of system failure.

Appendix I
Coefficients of the distance functions

Consider a distance function of the form (12), and the expression of the second-fundamental form in (10). The parameter $\lambda \in \mathbb{R}^m$ can be written $\lambda = [u \quad \zeta]^T$, with $u \in U \subset \mathbb{R}^k$ and $\zeta \in \mathbb{R}^l$ with $m = k + l$. Similarly, the approximation point around which the second-order approximation corresponding to the distance function was calculated can be written $\lambda_c = [u_c \quad \zeta_c]^T$.

Let $M = -\frac{1}{2} C \, \mathrm{d}N C^T$. Let the normal be $n(\lambda_c) = [n_1 \quad n_2]^T$ where $n_1 \in \mathbb{R}^k$ and $n_2 \in \mathbb{R}^l$ are the components of the normal corresponding to u and ζ in λ, respectively. Similarly, the matrix M can be written

$$M = \begin{bmatrix} (M)_{11} & (M)_{12} \\ (M)_{21} & (M)_{22} \end{bmatrix}, \tag{28}$$

where $(M)_{11} \in \mathbb{R}^{k \times k}$, $(M)_{12} = (M)_{21}^T \in \mathbb{R}^{k \times l}$ and $(M)_{22} \in \mathbb{R}^{l \times l}$. Let also $\Delta u = u - u_c$. Then the distance function can be written as a polynomial in ζ, see (14), with

$$\begin{aligned} a(u) =& (n_1)^T \Delta u + (\Delta u)^T M_{11} \Delta u + \\ & \left(n_2^T + 2(\Delta u)^T M_{12}\right) \zeta_c + \zeta_c^T M_{22} \zeta_c \end{aligned} \tag{29}$$

$$b_i = - n_2^T - 2M_{21}\Delta u - 2M_{22}\zeta_c \tag{30}$$

$$c_{ij} = M_{22} \tag{31}$$

Appendix II
Cumulants of the the distance functions

The first four cumulants $\kappa_{d,1}, \kappa_{d,2}, \kappa_{d,3}$ and $\kappa_{d,4}$ of a vector of p distance functions of the form (14) can be written as

$$\kappa_{d,1} = a^r + b_i^r \kappa^i + c_{ij}^r \kappa^{ij}. \tag{32}$$

$$\kappa_{d,2} = b_i^r b_j^s \kappa^{i,j} + b_i^r c_{jk}^s \kappa^{i,jk} + c_{ij}^r b_k^s \kappa^{ij,k} + c_{ij}^r c_{kl}^s \kappa^{ij,kl}. \tag{33}$$

$$\begin{aligned} \kappa_{d,3} =& b_i^r b_j^s b_k^t \kappa^{i,j,k} + b_i^r b_j^s c_{kl}^t \kappa^{i,j,kl} + b_i^r c_{jk}^s b_l^t \kappa^{i,jk,l} \\ &+ b_i^r c_{jk}^s c_{lm}^t \kappa^{i,jk,lm} + c_{ij}^r b_k^s b_l^t \kappa^{ij,k,l} + c_{ij}^r b_k^s c_{lm}^t \kappa^{ij,k,lm} \\ &+ c_{ij}^r c_{kl}^s b_m^t \kappa^{ij,kl,m} + b_{ij}^r b_{kl}^s b_{mn}^t \kappa^{ij,kl,mn}. \end{aligned} \tag{34}$$

$$\begin{aligned} \kappa_{d,4} =& b_i^r b_j^s b_k^t b_l^u \kappa^{i,j,k,l} + b_i^r b_j^s b_k^t c_{lm}^u \kappa^{i,j,k,lm} \\ &+ b_i^r b_j^s c_{kl}^t b_m^u \kappa^{i,j,kl,m} + b_i^r b_j^s c_{kl}^t c_{mn}^u \kappa^{i,j,kl,mn} \\ &+ b_i^r c_{jk}^s b_l^t b_m^u \kappa^{i,jk,l,m} + b_i^r c_{jk}^s b_l^t c_{mn}^u \kappa^{i,jk,l,mn} \\ &+ b_i^r c_{jk}^s c_{lm}^t b_n^u \kappa^{i,jk,lm,n} + b_i^r c_{jk}^s c_{lm}^t c_{no}^u \kappa^{i,jk,lm,no} \\ &+ c_{ij}^r b_k^s b_l^t b_m^u \kappa^{ij,k,l,m} + c_{ij}^r b_k^s c_l^t c_{mn}^u \kappa^{ij,k,l,mn} \\ &+ c_{ij}^r b_k^s c_{lm}^t b_n^u \kappa^{ij,k,lm,n} + c_{ij}^r b_k^s c_{lm}^t c_{no}^u \kappa^{ij,k,lm,no} \\ &+ c_{ij}^r c_{kl}^s b_m^t b_n^u \kappa^{ij,kl,m,n} + c_{ij}^r c_{kl}^s b_m^t c_{no}^u \kappa^{ij,kl,m,no} \\ &+ c_{ij}^r c_{kl}^s c_{mn}^t b_o^u \kappa^{ij,kl,mn,o} + c_{ij}^r c_{kl}^s c_{mn}^t c_{op}^u \kappa^{ij,kl,mn,op}. \end{aligned} \tag{35}$$

The quantities appearing in the expressions above are:

- $\kappa^{ij,k}, \kappa^{ij,kl,mn}, \ldots$: generalized cumulants of ζ. They can be computed from the ordinary cumulants [24, Chapter 3].
- a^r, b_i^r and c_{ij}^r are tensors whose elements are the $a(u)$, $b_i(u)$ and c_{ij} from (14) of the r-th distance function, $r =$

$1, \ldots, p$. For instance, c_{ij}^3 would correspond to c_{ij} from the third distance function, and $b_i^2(u)$ to $b_i(u)$ from the second distance function.

References

[1] M. Lauby, M. Ahlstrom, D. Brooks, S. Beuning, J. Caspary, W. Grant, B. Kirby, M. Milligan, M. O'Malley, M. Patel, R. Piwko, P. Pourbeik, D. Shirmohammadi, and J. Smith, "Balancing Act", *IEEE Power and Energy Magazine*, vol. 9, no. 6, pp. 75–85, Nov. 2011.

[2] I. Dobson, S. Greene, R. Rajaraman, C. L. DeMarco, F. L. Alvarado, M. Glavic, J. Zhang, and R. Zimmerman, "Electric Power Transfer Capability: Concepts, Applications, Sensitivity, Uncertainty", Power Systems Engineering Research Center, Technical report 01-34, Nov. 2001.

[3] A. Schellenberg, W. Rosehart, and J. Aguado, "Cumulant based stochastic optimal power flow (S-OPF) for variance optimization", in *IEEE Power Engineering Society General Meeting*, IEEE, 2005, pp. 2504–2509.

[4] H. Zhang and P. Li, "Probabilistic analysis for optimal power flow under uncertainty", *IET Generation, Transmission & Distribution*, vol. 4, no. 5, p. 553, 2010.

[5] M. Perninge and C. Hamon, "A Stochastic Optimal Power Flow Problem With Stability Constraints, Part II: The Optimization Problem", *IEEE Transactions on Power Systems*, pp. 1–1, 2012.

[6] C. Hamon, M. Perninge, and L. Soder, "A Stochastic Optimal Power Flow Problem With Stability Constraints, Part I: Approximating the Stability Boundary", *IEEE Transactions on Power Systems*, pp. 1–10, 2012.

[7] H. Bludszuweit, J. Dominguez-Navarro, and A. Llombart, "Statistical Analysis of Wind Power Forecast Error", *IEEE Transactions on Power Systems*, vol. 23, no. 3, pp. 983–991, Aug. 2008.

[8] B. Hodge, D Lew, M Milligan, and H Holttinen, "Wind Power Forecasting Error Distributions: An International Comparison", in *11th Annual International Workshop on Large-Scale Integration of Wind Power into Power Systems as well as on Transmission Networks for Offshore Wind Plants*, 2012.

[9] O. Alsac and B. Stott, "Optimal Load Flow with Steady-State Security", *IEEE Transactions on Power Apparatus and Systems*, vol. PAS-93, no. 3, pp. 745–751, May 1974.

[10] A. Monticelli, M. V. F. Pereira, and S. Granville, "Security-Constrained Optimal Power Flow with Post-Contingency Corrective Rescheduling", *IEEE Transactions on Power Systems*, vol. 2, no. 1, pp. 175–180, 1987.

[11] L. Sandberg and K. Roudén, "The real-time supervision of transmission capacity in the swedish grid", in *Real-time stability assessment in modern power system control centers*, S. C. Savulescu, Ed., First, Wiley-IEEE Press, 1992, ch. 11, pp. 279–306.

[12] M. Sobierajski, "Optimal stochastic load flows", *Electric Power Systems Research*, vol. 2, no. 1, pp. 71–75, Mar. 1979.

[13] T. Yong and R. Lasseter, "Stochastic optimal power flow: formulation and solution", in *2000 Power Engineering Society Summer Meeting*, vol. 1, IEEE, 2000, pp. 237–242.

[14] C. Hamon, "On Frequency Control Schemes in Power Systems with Large Amounts of Wind Power", Licentiate Thesis, KTH, 2012.

[15] T. Van Cutsem and C. D. Vournas, "Voltage stability analysis in transient and mid-term time scales", *IEEE Transactions on Power Systems*, vol. 11, no. 1, pp. 146–154, 1996.

[16] I. Dobson and H.-D. Chiang, "Towards a theory of voltage collapse in electric power systems", *Systems & Control Letters*, vol. 13, no. 3, pp. 253–262, Sep. 1989.

[17] I. Dobson and L. Lu, "Voltage collapse precipitated by the immediate change in stability when generator reactive power limits are encountered", *IEEE Transactions on Circuits and Systems I: Fundamental Theory and Applications*, vol. 39, no. 9, pp. 762–766, 1992.

[18] I. Dobson, "An iterative method to compute a closest saddle node or Hopf bifurcation instability in multidimensional parameter space", in *[Proceedings] 1992 IEEE International Symposium on Circuits and Systems*, vol. 5, IEEE, 1992, pp. 2513–2516.

[19] M. E. Karystianos, N. G. Maratos, and C. D. Vournas, "Maximizing Power-System Loadability in the Presence of Multiple Binding Complementarity Constraints", *IEEE Transactions on Circuits and Systems I: Regular Papers*, vol. 54, no. 8, pp. 1775–1787, Aug. 2007.

[20] M. Perninge and L. Söder, "Optimal distribution of primary control participation with respect to voltage stability", *Electric Power Systems Research*, 2010.

[21] ——, "On the Validity of Local Approximations of the Power System Loadability Surface", *IEEE Transactions on Power Systems*, vol. PP, no. 99, pp. 1–1, Mar. 2011.

[22] M. Perninge, "Approximating the loadability surface in the presence of SNB–SLL corner points", *Electric Power Systems Research*, vol. 96, pp. 64–74, Mar. 2013.

[23] A. Pressley, *Elementary differential geometry*. Springer Verlag, 2010.

[24] P. McCullagh, *Tensor Methods in Statistics*. Chapman and Hall, 1987.

[25] I Griva, S. Nash, and A Sofer, "Linear and nonlinear optimization", 2009.